IEEE Access
Multidisciplinary | Rapid Review | Open Access Journal

SPECIAL SECTION ON TUNABLE DEVICES FOR MODERN COMMUNICATIONS: MATERIALS, INTEGRATION, MODELING, AND APPLICATIONS

Received November 22, 2017, accepted December 20, 2017, date of publication January 3, 2018, date of current version March 9, 2018.

Digital Object Identifier 10.1109/ACCESS.2017.2789199

Advances in Reconfigurable Antenna Systems Facilitated by Innovative Technologies

Y. JAY GUO[1], (Fellow, IEEE), PEI-YUAN QIN[1], (Member, IEEE), SHU-LIN CHEN[1], (Student Member, IEEE), WEI LIN[1], (Member, IEEE), AND RICHARD W. ZIOLKOWSKI[1,2], (Fellow, IEEE)

[1]Global Big Data Technologies Centre, University of Technology Sydney, Ultimo, NSW 2007, Australia
[2]Department of Electrical and Computer Engineering, The University of Arizona, Tucson, AZ 85721, USA

Corresponding author: Pei-Yuan Qin (peiyuan.qin@uts.edu.au)

This work was supported by the Australia Research Council Discovery Program under Grant DE170101203 and Grant DP160102219.

ABSTRACT Future fifth generation (5G) wireless platforms will require reconfigurable antenna systems to meet their performance requirements in compact, light-weight, and cost-effective packages. Recent advances in reconfigurable radiating and receiving structures have been enabled by a variety of innovative technology solutions. Examples of reconfigurable partially reflective surface antennas, reconfigurable filtennas, reconfigurable Huygens dipole antennas, and reconfigurable feeding network-enabled antennas are presented and discussed. They represent novel classes of frequency, pattern, polarization, and beam-direction reconfigurable systems realized by the innovative combinations of radiating structures and circuit components.

INDEX TERMS Beam steering, feeding networks, polarization, reconfigurable antennas, radiation patterns.

I. INTRODUCTION

Wireless systems are evolving towards multi-functionality to enable fast, secure, and reliable communications. This feature catalyzes competitive advantages for a large number of civilian and military applications from providing high data-rate wireless access in congested environments along with highly-secure data transmissions to equipping mobile platforms with enabling and innovative wireless solutions. To reach their full potential, these highly intelligent systems require not only adaptive signal processing techniques, but also revolutionary hardware. Antennas, which are one of the key enabling components, play a critical role in determining a wireless system's ultimate performance [1]. Traditional antennas, whose characteristics are fixed for specific functionalities, severely limit the level of intelligence that can be introduced into multi-functional wireless systems. Consequently, the realization of multi-functional antennas is a fundamental challenge for future wireless systems. Recently reported reconfigurable antenna (RA) technologies are emerging as promising solutions; they provide sufficient flexibility and adaptability to fast changing wireless system requirements and their operational environments.

Taking the upcoming fifth generation (5G) communication systems as an example, 5G networks will rely heavily on cognitive radio (CR) strategies to achieve their promised extremely high data rates and low latency. They are facilitated by CR technologies that sense variations occurring in the wireless environment, and then adapt their parameters to achieve optimal transmissions. The cognitive radio, which is a particular type of multi-functional wireless system, leverages the combinations of frequency agility, polarization adaptability, and pattern diversity, as well as adaptive signal processing and network protocols, to accomplish the anticipated 5G requirements [2]. There are no doubts that RAs rather than conventional antennas must be employed to facilitate the realization of CR systems and their expected features.

Furthermore, the numbers of antennas that will be needed and placed on many future civilian and military wireless platforms will be significant. The mutual couplings between all of these antennas can cause detrimental electromagnetic interference (EMI) and electromagnetic compatibility (EMC) problems ranging from temporary disruption of the system performance to permanent equipment damage. Simultaneously, there are severe space, weight, and cost limitations associated with the desire and need for compact mobile platforms. Conventional antenna systems and their large volumes and significantly complex feed structures simply cannot meet

these demands. Again, RAs can be used to significantly reduce the number of antennas necessary for wireless systems, as well as to mitigate any EMI and EMC problems. Consequently, they have the great potential to enhance the reliability of future wireless platforms.

In the last decade, there have been significant advances in RAs, focusing on the antenna performance characteristics of frequency, polarization, radiation pattern, and combinations of these parameters. Depending on their mechanisms to tailor these characteristics, RA developments can be classified into three main types, namely, employing electrical devices, such as PIN diodes, radio frequency (RF) micro-electromechanical systems (RF-MEMS), and varactor diodes; employing mechanical changes; and employing material changes. Several books and book chapters [3]–[5] are available that provide extensive literature reviews on the current state-of-the-art in RAs. In contrast, we summarize in this article several recent emerging technologies that lead to advanced RAs. These include reconfigurable partially reflective surfaces (PRSs), reconfigurable filtennas, reconfigurable Huygens antennas, and reconfigurable feeding network technologies. They will be discussed, respectively, in Sections II, III, IV, and V. It is expected the technologies discussed can be employed to design other RAs with various specifications.

II. RECONFIGURABLE PARTIALLY REFLECTIVE SURFACE (PRS) ANTENNAS

To extend the communications range and to achieve high data rates, moderate/high-gain reconfigurable antennas (RAs) are highly desirable for many wireless communication systems. Partially reflective surface (PRS) antennas, also known as Fabry-Pérot (FP) antennas, usually employ a source antenna with low directivity and a broad beamwidth, and a metallic or metallodielectric periodic array attached to a superstrate. The array is located approximately half a wavelength above the source [6], [7], beneath the superstrate. The combination of the array and the superstrate is typically denoted as the PRS. Electromagnetic waves radiated from the source experience multiple reflections and transmissions within the FP cavity, i.e., the cavity formed by the ground plane and the superstrate [6]. The waves transmitted through the PRS will be in phase [7] when certain resonance conditions are satisfied, thus enhancing the directivity of the antenna. A PRS antenna has the advantages of being low profile and simply constructed, and having high gain. Compared with array antennas, a feeding network, which can become very lossy for large arrays, is not needed. On the other hand, a significant drawback of a standard PRS antenna is its narrow operating bandwidth which is a consequence of the high Q factor of the FP cavity. Furthermore, traditional PRS antennas radiate fixed radiation patterns with fixed polarizations. Recently, various reconfiguration technologies have been developed to enable PRS antennas to dynamically change the operating frequency [8], polarization [9], [10], and the radiation pattern [11]–[13].

A. FREQUENCY RECONFIGURABLE PRS ANTENNAS

The typical half-wavelength profile of a PRS antenna can be reduced [14], [15] using a high impedance surface (HIS) to replace the ground plane. Moreover, a frequency reconfigurable PRS antenna has been reported that increases its operating bandwidth by employing a tunable HIS [8]. This system consists of a stacked patch-fed antenna, a PRS, and a reconfigurable high impedance surface (HIS). Varactor diodes are soldered onto each cell of the HIS. By changing the voltages applied to them, the reflection phases of the HIS can be changed. Because its operating frequency is a function of the reflection phases of both the PRS and HIS, as well as the height of the PRS above the ground plane, the controlled variations of those HIS reflection phases alone are sufficient to facilitate the frequency reconfiguration of the antenna.

B. PATTERN RECONFIGURABLE PRS ANTENNAS

Most of the reported pattern reconfigurable antennas [16]–[21] have concentrated on the reconfiguration of a single radiator (or using switches to select one radiator among a few). This choice arises from the ease of implementing the biasing networks and the consequent validation of the design concepts. However, because only a single radiator is reconfigured, the realized gains of those antennas are rather low. Several technologies have been reported that achieve pattern reconfigurable PRS antennas with moderate/high gains.

A PRS antenna fed at the center of the cavity generally radiates a broadside beam. Two methods are usually used to tilt the beam at a fixed operating frequency. The first one employs a phase-changing metamaterial surface as the PRS to achieve a variable reflection phase distribution. For example, a PRS antenna proposed in [11] has a maximum beam tilt of 20° with respect to the broadside. By varying the value of the capacitance of the PRS structure, its output beam at 7.9 GHz was rendered electronically steerable through $\pm 7°$ by using varactor diodes [12]. The second way to realize beam steering is to employ a phased antenna array as the radiating source for the PRS antenna. For instance, a two-element antenna array consisting of Wilkinson power dividers and phase shifters was developed in [13] to excite the PRS in order to tilt the beam. Beam scanning from $-10°$ to $+10°$ was realized at 2.0 GHz. Furthermore, by incorporating a separate reconfigurable matching network, an impedance bandwidth of 3% (range of frequencies in which the operational bands of all the beams overlap) was obtained.

Additionally, it is noted that research work has been conducted to realize a fixed-frequency beam scanning of one-dimensional (1D) leaky-wave antenna using a reconfigurable HIS [22]. The reported antenna provides continuous electronic beam scanning at 5.5 GHz in the angular range from $-25°$ to $25°$. This pattern reconfiguration method has been extended to a two-dimensional (2D) PRS antenna that can achieve beam scanning in both the elevation and azimuth planes [23], [24]. However, the antenna's aperture efficiency

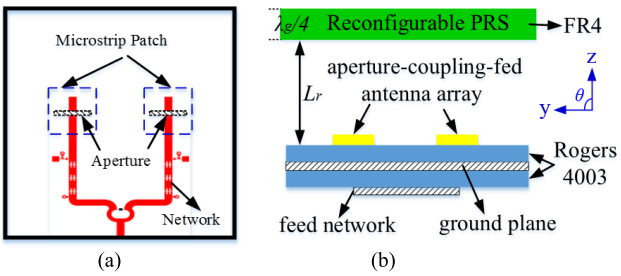

FIGURE 1. PRS antenna with array feeding source. (a) Top view. (b) Side view [25].

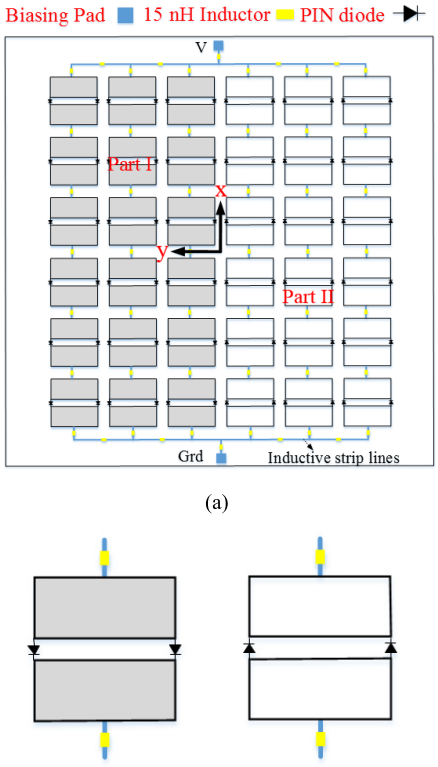

FIGURE 2. Reconfigurable PRS structure. (a) Layout. (b) Unit cells with their PIN diodes and biasing lines [25].

is quite low since only part of the antenna is utilized for radiation at any given time.

A pattern reconfigurable PRS antenna was presented in [25] that employed a novel non-uniform reconfigurable PRS structure which was driven by a 2-element phased array to achieve the desired beam-steering. The antenna is capable of switching the main beam directions among the angles: $-15°$, $0°$, and $15°$, in an overlapping frequency bandwidth that is from 5.5 to 5.7 GHz (4.0% fractional impedance bandwidth). The realized gain of the antenna is over 12 dBi. The schematics of this reconfigurable PRS antenna are given in Fig. 1.

The reconfigurable PRS itself is shown in Fig. 2. The PRS is divided into the two parts with respect to the center of the

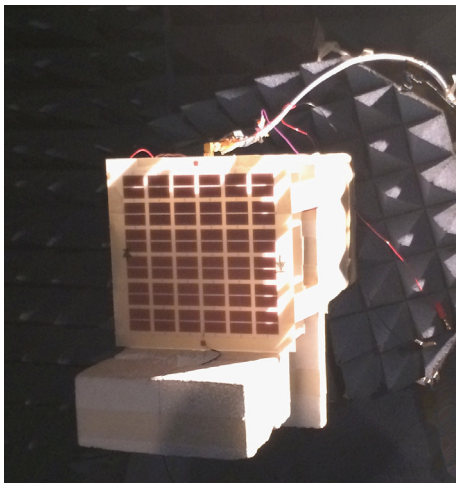

FIGURE 3. Prototype of the reconfigurable PRS antenna under test conditions [25].

structure. Each part consists of 3×6 tunable cells. For each cell, a 20.5 mm $\times$ 20.5 mm microstrip patch with a slot in the center is printed on a 0.8-mm-thick FR4 substrate ($\varepsilon_r = 4.4$, $\mu_r = 1.0$, $\tan\delta = 0.018$). For each cell, two PIN diodes are soldered in the middle of the patch. By controlling the diodes, the phase of the input reflection coefficient of each cell can be changed, thereby producing a reflection phase difference between the two parts of the PRS structure. As a result, the output beam direction can be switched. When the PIN diodes are turned off, the patch has a high reflectivity with a small phase. When the PIN diodes are turned on, a larger value of the phase is obtained. When the two sets (halves) of the PIN diodes are in opposite states, a progressive phase shift is achieved across the PRS structure, thereby realizing a tilted beam.

In order to increase the tilt range of the PRS antenna without an increase in the side lobe level, a phased array can be employed as its source (exciter). To acquire the required phase shifts between the array elements, phase shifters based on reconfigurable defected microstrip structure (RDMS) [26] are employed as shown in Fig. 1 (a). The feeding network consists of two phase shifters. Each phase shifter consists of three identical RDMS units integrated with PIN diodes, etched on one branch of the Wilkinson power divider. Each RDMS unit can generate a $30°$ phase delay in this design. Thus, by cascading three RDMS units, a full $90°$ phase shift can be obtained.

Fig. 3 shows the photograph of the PRS antenna prototype. The measured H-plane (y-z plane) radiation patterns of the antenna for three states are shown in Fig. 4. It is seen that broadside radiation is realized for State 1. The beam directions are steered towards $-15°$ and $15°$ from broadside for State 2 and State 3, respectively.

C. POLARIZATION RECONFIGURABLE PRS ANTENNAS

The antennas reported that achieve polarization reconfigurability generally can be switched between LP states and/or

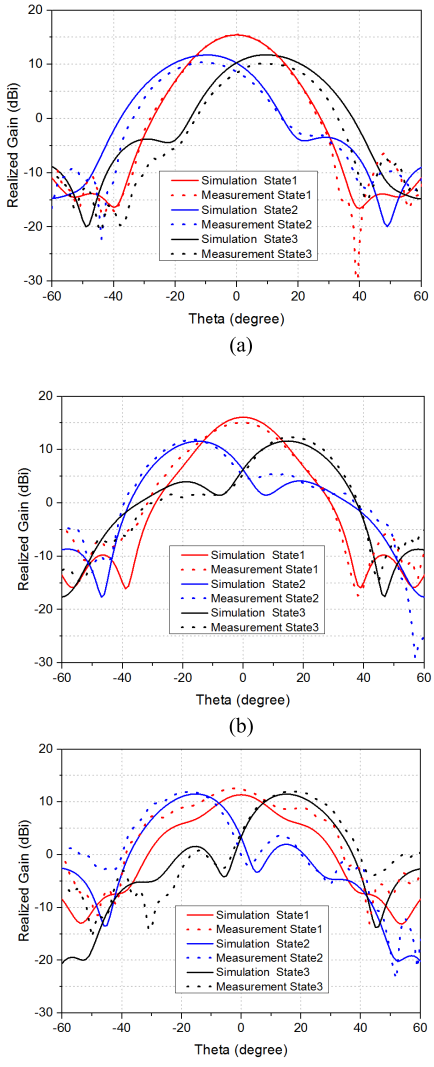

FIGURE 4. The patterns of the realized gain at (a) 5.3GHz, (b) 5.5GHz, and (c) 5.7GHz [25].

two CP states [27]–[31]. It is found that most examples have an overlapping impedance bandwidth of their two states that is less than 10%. Furthermore, if they are of the CP type, then their CP bandwidth is determined more accurately by the overlap of the impedance and the axial ratio (AR) bandwidths. The available examples then have even narrower bandwidths. Consequently, it is noted that realizing wide bandwidths is a serious challenge for polarization agile systems.

There have been notable successes. For instance, a wheel-shaped polarization agile antenna was proposed in [31] that can achieve a 28.6% (3.45 to 4.6 GHz) impedance bandwidth and 15.4% axial ratio bandwidth. Furthermore, most reported polarization reconfigurable designs employ only a single microstrip patch; hence, their realized gains are very limited. On the other hand, the polarization reconfigurable antenna array presented in [32] can switch between two orthogonal

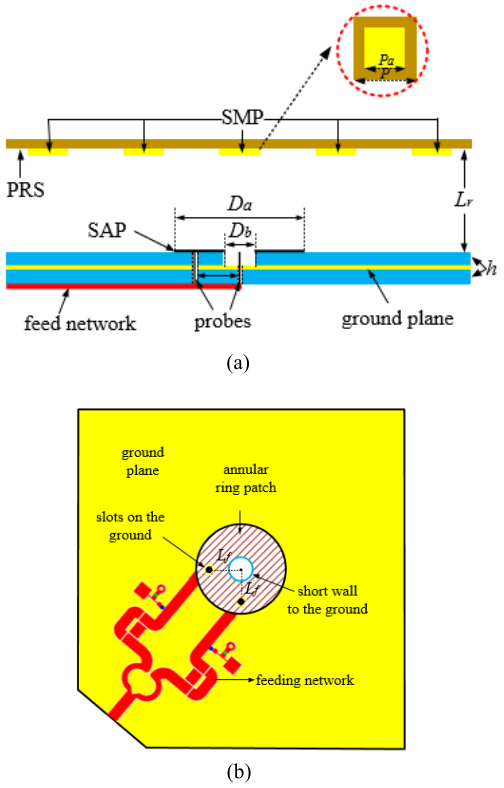

FIGURE 5. Schematics of a polarization reconfigurable PRS structure. (a) Side view; (b) Top view of the source [34].

±45° linear polarizations with a maximum gain of 13.5 dBi. One way to further increase the gain is to introduce a PRS structure as the superstrate. For example, the PRS polarization reconfigurable antenna presented in [33] employs a microstrip patch antenna with switchable slots as the source. Either right hand circular polarization (RHCP) or left hand circular polarization (LHCP) can be radiated by controlling the status of the switches. A 1.5% CP bandwidth was achieved with a simulated realized gain of 21 dBi.

A novel wideband PRS antenna was proposed in [34] which can change its polarization between linear polarization (LP), LHCP, and RHCP electronically. A measured 13.1% CP fractional bandwidth from 4.7 to 5.36 GHz is achieved. The antenna has a realized gain of around 9 dBi / dBic for the different polarization states.

Fig. 5 shows the design of the polarization reconfigurable PRS antenna reported in [34]. As illustrated in Fig. 5 (a), it is composed of a PRS structure, a shorted annular patch (SAP) antenna located above the ground plane as the source, and a reconfigurable feeding network located underneath the ground plane. The dimensions of the antenna are 110 mm × 110 mm (1.83λ × 1.83λ at 5 GHz). The PRS consists of 5 × 5 square metallic patches printed on a 0.8 mm thick FR4 substrate ($\varepsilon_r = 4.4, \mu_r = 1.0, \tan\delta = 0.018$). The SAP antenna is selected as the source antenna with a diameter of 1.3 mm. It is fed by two probes as shown in Fig. 5 (b). When the phase difference between the two feed probes is 90°,

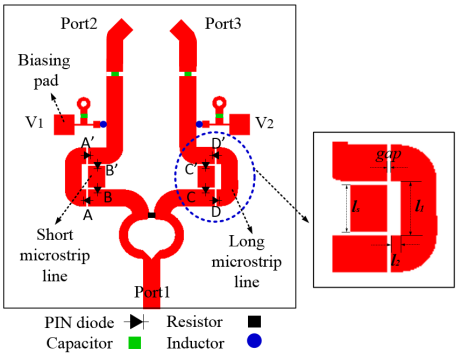

FIGURE 6. Schematic of the feeding network for the polarization RA [34].

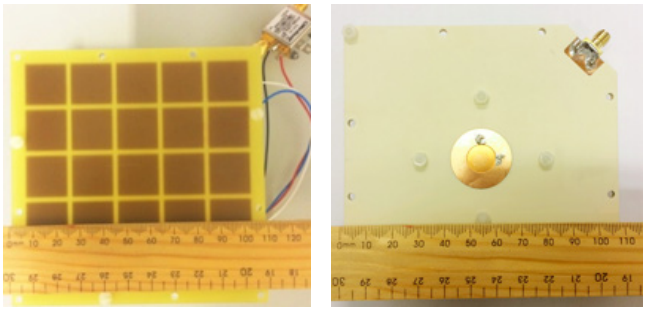

FIGURE 7. Photographs of the polarization reconfigurable PRS antenna prototype. (a) With the PRS structure. (b) Without the PRS structure [34].

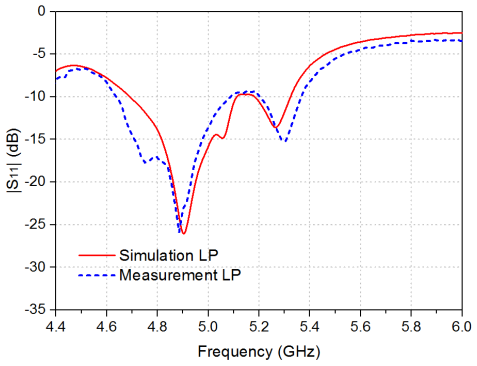

FIGURE 8. Comparison of the measured and simulated $|S_{11}|$ values of the reconfigurable PRS antenna in its LP state [34].

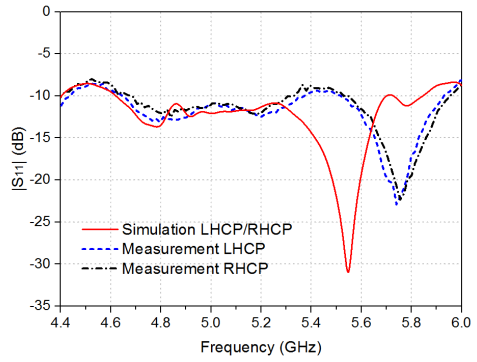

FIGURE 9. Comparison of the measured and simulated $|S_{11}|$ values of the reconfigurable PRS antenna in its CP states [34].

circular polarization can be realized [35]. The radiating source is a two-layer structure. For the first layer, the SAP antenna is printed on the upper side of a 1.524-mm-thick Rogers 4003 substrate ($\varepsilon_r = 3.55$). The metal of the other side of the substrate is kept as the ground plane. For the second layer, a reconfigurable feeding network is printed on the bottom side of another 1.524-mm-thick Rogers 4003 substrate. The metal of the top side of this substrate is removed. Two metal probes are employed to connect the SAP antenna and the feeding network. The probes are separated from the ground by etching two circular slots around them.

To realize polarization reconfiguration between the LP and CP states, a reconfigurable feeding network was designed. Fig. 6 shows the structure of the network. It consists of a conventional Wilkinson power divider and a phase shifter inserted on each branch. The phase shifter given in the inset consists of a long and a short microstrip line. PIN diodes are placed at the gaps of each line. The short microstrip lines are about $\lambda g/4$ shorter than the long ones, where λg is the guided wavelength at the resonant frequency. By switching the diodes between different states, the electrical length of each branch of the power divider can be changed. As a result, phase differences between the two output ports can be produced, thereby achieving polarization reconfiguration. The feeding network has four groups of PIN diodes: A and A'; B and B'; C and C'; D and D'. When A, A' and D, D' are turned on and the others are off, there is no phase difference between the two branches. This state is named S1 in this paper. When A, A' and C, C' are turned on while the others are turned off, the phase of the left branch is 90° behind that of the right one. This state is named S2. When B, B' and D, D' are turned on with the others off, this state S3 has a 90° phase lead in the left branch. In this manner, the antenna driven by this feeding network can realize polarization switching among the LP (S1), LHCP (S2) and RHCP (S3) states.

Photos of the prototype that was fabricated and measured are given in Fig. 7. The measured $|S_{11}|$ values shown in Figs. 8 and 9 indicate that the 10-dB impedance bandwidth is from 4.65 to 5.36 GHz for the LP mode and from 4.63 to 5.95 GHz for the LHCP and RHCP modes. The comparisons with the simulated values show very good agreement. The simulated and measured axial ratio (AR) values for the CP modes are given in Fig. 10. The measured AR values are below 3 dB for both the LHCP and RHCP states from 4.7 to 5.38 GHz (13.5%). The overlapping impedance and AR frequency bandwidth is from 4.7 to 5.36 GHz (13.1%). The antenna has average realized gains of about 9 dBi / dBic.

III. RECONFIGURABLE FILTENNAS

One of the highly regarded technologies that has the promise to enhance the spectrum efficiency is Cognitive Radio (CR) [36]. An intelligent CR system can sense and

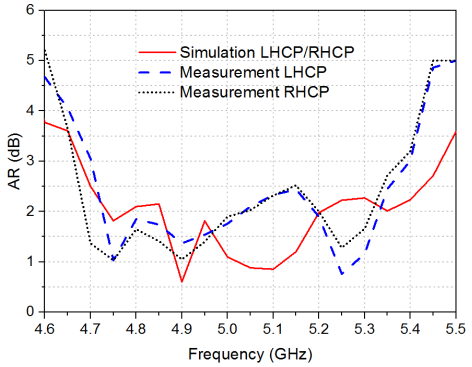

FIGURE 10. Comparison of the measured and simulated axial ratio (AR) values of the reconfigurable PRS antenna [34].

learn the channel activities and then select the optimal communication strategies. Choices include the radiation characteristics, modulation schemes, and network topologies. One CR strategy is to change the operating frequency of the system. Specifically, by sensing the spectrum usage, a CR system can then avoid causing interference with other users by allocating services to an unoccupied part of the spectrum. Consequently, a typical suggestion is to require two separate antennas to obtain this functionality. In particular, a wideband antenna would be assigned to scan the spectrum; and a reconfigurable antenna (RA) having a narrow frequency bandwidth would be dedicated for the communication assignments.

RAs that focus on narrowband frequency tuning have been investigated extensively for several decades [37]–[40]. These systems include dipole antennas and microstrip patch antennas, to name a few. By using a single-port fed antenna that can switch between the wideband and narrowband operational states, researchers have shown that one can combine the two desired antenna types together. The end result is a reduction in the size and complexity of the CR system's RF front-end. For instance, a microstrip monopole antenna has been developed [41] that achieves an ultra-wideband (UWB) state, and a state in which three narrow bands are available. Two GaAs field effect transistor (FET) switches are employed to control the connections between the different stubs and the main feed line of the monopole and, thus, to achieve the desired narrowband frequency reconfiguration. Another example is a Vivaldi antenna capable of switching between its wideband and six discrete narrowband states [42]. The design was accomplished by inserting two ring slots into the feeding area of the Vivaldi element that were loaded with fifteen PIN diodes. Switching these diodes on or off served to create different resonators and, hence, to realize distinct, reconfigurable narrowband operational states.

Another useful CR technology is the introduction of a reconfigurable filter into the antenna system. In particular, a reconfigurable filter-antenna has been realized that also can switch between its wideband and frequency agile narrowband operational states. It consists of a bandpass filter that is integrated directly into the feed line of the antenna [43].

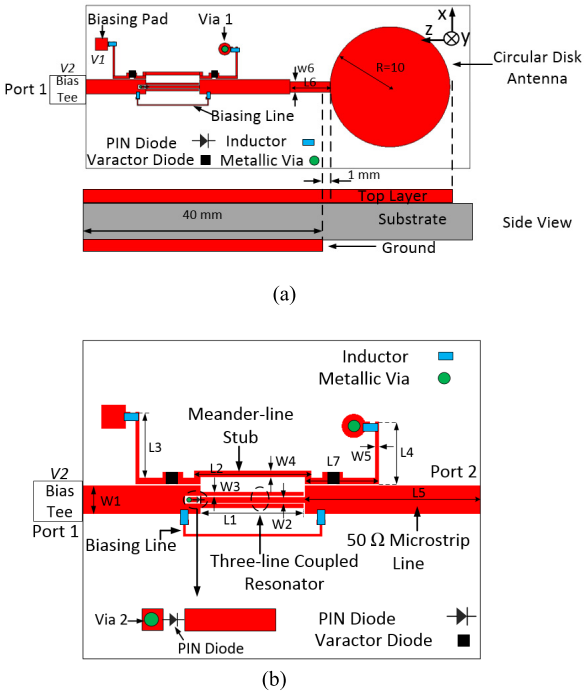

FIGURE 11. Reconfigurable filter-antenna [43]. (a) Top and side views. (b) Layout of the TLCR filter integrated with a 50-Ω microstrip feedline [43].

This reconfigurable filter is based on a three-line coupled resonator (TLCR). Simply switching between its wide and narrow bandpass responses with a PIN diode, one can reconfigure the antenna system to operate in either its wideband or narrowband state. Furthermore, two varactor diodes are introduced to enable the continuous reconfiguration of the operating frequency of its narrowband state.

This reconfigurable filter-antenna is depicted in Fig. 11 (a). Its elements are printed on the two sides of a 0.787-mm-thick RT/Duroid^{TM} 5880 substrate ($\varepsilon_r = 2.2$, $\mu_r = 1.0$, and $\tan\delta = 0.0009$). The top layer consists of a circular disc that acts as the radiating element and the TLCR-based bandpass filter integrated with a 50-Ω microstrip feedline. The radius of this circular disc monopole antenna is 10 mm. This filter-antenna achieves a very wide −10-dB impedance bandwidth.

The TLCR filter configuration is illustrated in Fig. 11 (b). It includes an input/output 50-Ω microstrip line, a meander-line stub, and the diodes and their biasing circuits. The desired bandpass response was realized [44] by adjusting the impedance of the three high-impedance lines and the distance between them (0.15 mm). A PIN diode and a metallic via (via 2) connects the middle high impedance line to the ground. The filter has a wide bandpass performance and the antenna operates in its wideband state when the diode is switched off. The filter has a narrow bandpass performance and the antenna operates in its narrowband state when the diode is turned on, i.e., the middle high-impedance line is shorted to the ground. The meander-line stub, which is located 0.15 mm above the 50-Ω microstrip lines, is the main producer of the energy

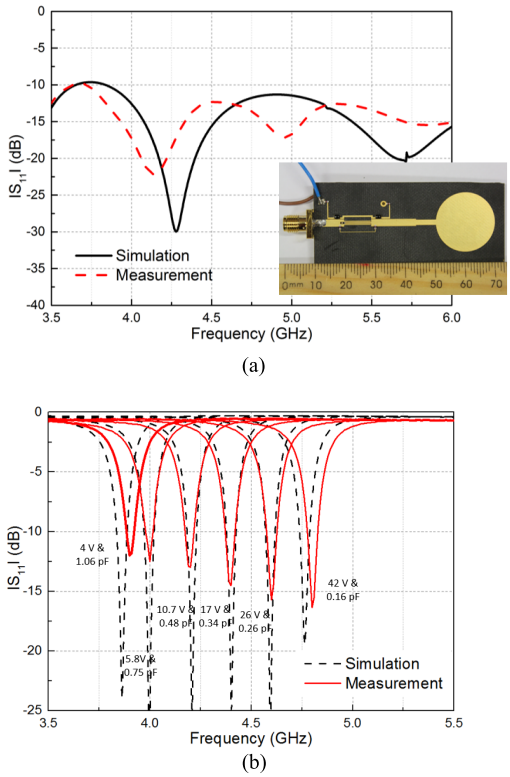

FIGURE 12. Simulated and measured $|S_{11}|$ values versus the source frequency when the reconfigurable-filter antenna is in its (a) wideband state, and (b) narrowband state [43].

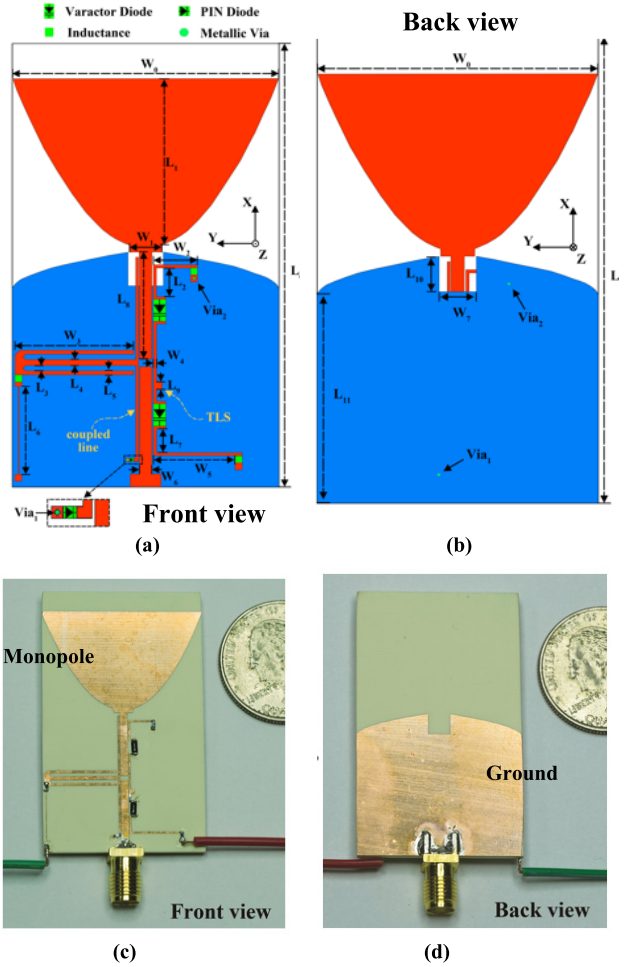

FIGURE 13. Frequency-reconfigurable filtenna. (a) Front and (b) back views of the HFSS model. (c) Front and (d) back views of the fabricated prototype [45].

coupling between Port 1 and Port 2. With the placement of two varactor diodes into appropriate positions on the stub, its electrical length can be varied. This feature facilitates tuning the center frequency of each narrow frequency band.

The measured and simulated input reflection coefficients for the wideband and narrowband states are shown in Figs. 12 (a) and (b), respectively. A photograph of the fabricated antenna prototype is shown in the inset of Fig. 12 (a). The varactor diodes yield 0.2 pF in their off states and produce an acceptable impedance match for the corresponding wideband state. The measured −10-dB impedance bandwidth shown in Fig. 12 (a) covers a wide frequency range from 3.8 to 6.0 GHz. On the other hand, when the diodes are turned on, the antenna works in its narrowband state. Fig. 12 (b) illustrates that the measured (simulated) operating frequencies of these narrow bands have a 1.24 tuning ratio, i.e., the system can be tuned continuously from 3.9 to 4.82 GHz (3.85 to 4.76 GHz) by varying the reversed bias voltage from 4.0 V to 42.0 V.

The integration of a filter directly into an antenna structure has led to the "filtenna" descriptor. Very similar to the preceding system, a frequency-reconfigurable filtenna for CR applications [45] was achieved by integrating a wideband, reconfigurable bandpass filter [46], [47] into a wideband funnel-shaped monopole antenna. This compact filtenna exhibits sharp out-of-band rejection in both its wideband and continuously tunable narrowband states. Fig. 13 shows the HFSS model and photos of the fabricated prototype. The frequency range of the wideband sensing state is from 2.35 to 4.98 GHz. The narrow band states cover communications within the 3.05 to 4.39 GHz range. These operational bands completely encompass the WiMAX band and the satellite communications C-band. A PIN diode is employed to switch between them. Two varactor diodes are used to shift the operational frequencies continuously among the narrowband states. The measured reflection coefficients, radiation patterns, and realized gains for both operational states were in good agreement with their simulated values [45].

While monopoles are well-known UWB radiators, it was the progression from the design of the compact frequency-reconfigurable filter illustrated in Fig. 14 and the principles to integrate it effectively with the monopole that enabled the filtenna. This reconfigurable filter is composed mainly of a C-shaped narrowband resonator [46], an E-shaped wideband resonator [47], two parallel-coupled transmission lines, and a 50-Ω input/output microstrip line. It was engineered to be realized with standard, printed circuit board (PCB) technology and the Rogers 4350B substrate ($\varepsilon_r = 3.48$, $\mu_r = 1.0$,

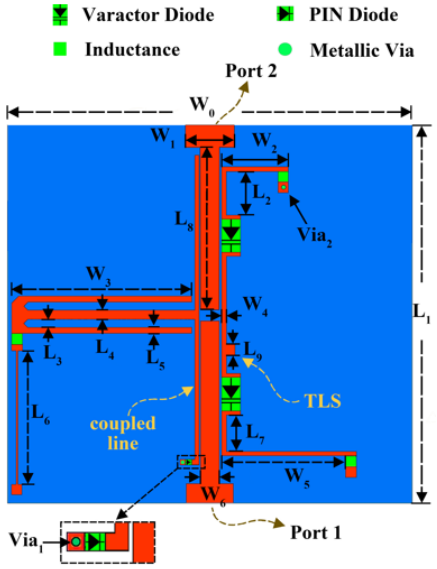

FIGURE 14. The layout of the compact, wideband, frequency-reconfigurable bandpass filter [45].

and $\tan\delta = 0.0038$). A 50-Ω microstrip transmission line connects the input and output ports, and is directly connected to the ground via a PIN diode integrated with (metallic) Via1. It is capacitively-coupled to the E-shaped wideband resonator, which is located halfway between those ports.

The reconfigurable filter operates between its wideband and narrowband states simply by switching the PIN diode, which is placed at the end of the coupled line close to the Port, to its OFF or ON state. The diode acts as a resistor (capacitor) when operating in its ON (OFF) state. The DC bias line for this diode is positioned at the bottom left side in Fig. 14. A RF-blocking coil inductor is connected to one end; the other end is connected the left side of the E-shaped resonator. This position minimizes its influence on the filter performance.

The C-shaped narrowband resonator is located on the right side of the input/output line. One end is connected to ground through another blocking inductor integrated with a (metallic) via (Via2). The other end, near Port 1, is connected to a DC bias pad through another inductor. Varactor diodes are inserted into the coupled-line sections of this C-shaped resonator. They act as series RLC equivalent circuits. The tuning reverse bias voltage of each diode can be varied from 20.0 to 2.0 V, which changes the junction capacitance Cj in the range from 0.1 to 1.0 pF. When the PIN diode is turned OFF (ON), the composite filter operates in its wideband state (narrow band states). The power reaching port 2 from port 1 in the narrowband states is transmitted mainly through the C-shaped narrowband resonator. One can then continuously shift the filter's narrowband operational frequencies across the entire spectrum of the wideband state simply by varying the voltages applied to the two varactor diodes.

The measured and simulated $|S_{11}|$ values for both operational states are shown in Fig. 15. The measured (simulated)

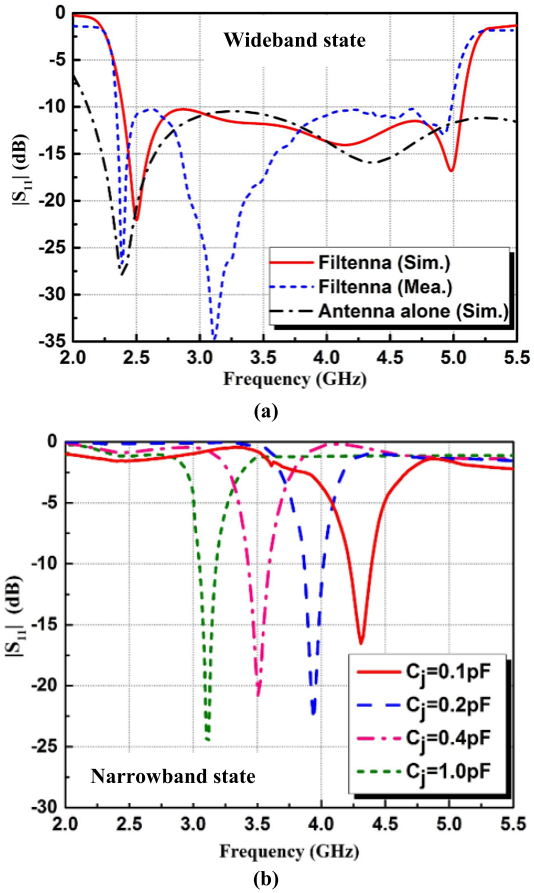

FIGURE 15. Measured and HFSS-predicted $|S_{11}|$ values as functions of the source frequency when the filtenna is operating in its (a) wideband state and in its (b) narrow band states [45].

−10-dB impedance bandwidth is 2.63 GHz (2.70 GHz), from 2.35 (2.40) to 4.98 GHz (5.10 GHz), yielding a 71.76% (72.0%) fractional bandwidth in its wide band state. Similarly, its narrowband states exhibit quite sharp passbands ranging from 3.05 (3.12) to 4.39 (4.44) GHz, i.e., they cover a 1.34 (1.32) GHz bandwidth. Thus, the measured (simulated) fractional bandwidth of this frequency-agile range reaches as high as 36.0% (34.9%).

IV. RECONFIGURABLE HUYGENS ANTENNAS

The introduction of near-field resonant parasitic (NFRP) elements based on metamaterial-inspired structures has facilitated the realization of efficient, multi-functional electrically small antenna systems (ESAs) [48]. By embedding a variety of circuit elements into these NFRP elements, frequency tunable (frequency agile antennas, e.g. with varactors [49]–[51]), wireless power transfer (rectennas, i.e., with rectifiers [52], [53]), and even broad bandwidth and beamwidth (with non-Foster elements [54]–[58]) systems have been designed, fabricated, and tested successfully. Moreover, by combining electric and magnetic NFRP elements [59]–[63] augmented with non-Foster circuits [64], [65], efficient, broad bandwidth, high directivity with large front-to-back ratio (FTBR) ESAs have been

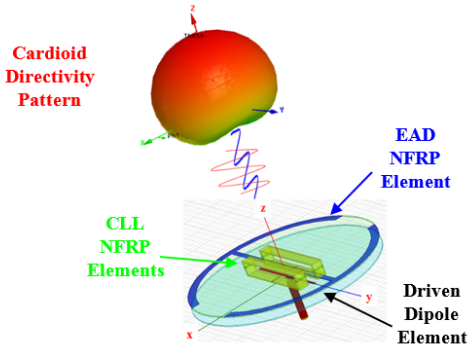

FIGURE 16. Geometry of Huygens dipole ESA formed by a combination of electric (EAD) and magnetic (CLL) NFRP elements [60].

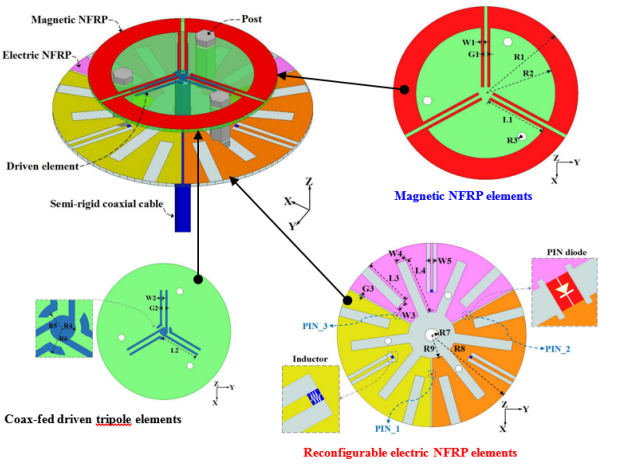

FIGURE 17. HFSS model of the pattern-reconfigurable, low profile, electrically small, Huygens dipole antenna design. The subplots display (in a clock-wise direction) an isometric view of the multi-layer structure and top views of the magnetic NFRP elements, the reconfigurable electric NFRP elements, and the driven tripole elements [66].

realized. By introducing switches, a pattern-reconfigurable ESA design and prototype, which verified its operating principles, that covers the entire azimuthal plane has been reported [66].

The basic broadside radiating Huygens dipole antenna system is depicted in [60, Fig. 16]. This NFRP design is low profile (height approximately $\lambda/80$) and electrically small ($ka = 0.45$). It radiates near 300 MHz with high radiation efficiency and a high FTBR. It consists of two electrically small, metamaterial-inspired NFRP elements excited by a coax-fed dipole antenna. The electric dipole response is obtained by spatially loading the driven dipole with a tunable Egyptian axe dipole (EAD) NFRP element. A magnetic dipole response is obtained by spatially loading the driven dipole with tunable, capacitively loaded loop (CLL) NFRP elements. At its resonance frequency, 299.17 MHz, the total radiated (accepted) power is AP = 0.98 (RP = 0.89) W, giving a radiation efficiency RE = 90.5%. The maximum directivity is $D_{max} = 5.05$ dB and the FTBR = 24.50 dB. The peak realized gain $RG_{max} = 4.53$ dB.

Linear polarized (LP) versions of this broadside radiating Huygens dipole antenna concept have been realized at 1.5 [61] and at 28 GHz [62]. A circularly polarized (CP) version has been realized at 1.575 GHz [63]. A non-Foster augmented LP version at 1.58 GHz has also been reported [65].

These NFRP element results led to the realization of a pattern-reconfigurable antenna [66]. Its HFSS model is shown in Fig. 17. The design again incorporated both electric and magnetic NFRP dipole elements. A set of three Huygens sources were attained, each covering a 120° sector, by arranging these electric and magnetic NFRP elements properly. Three 120° sectoral magnetic CLL elements lie on the top surface of the top disk. Three 120° sectoral electric NFRP elements lie on the top surface of the lower disk. These copper regions are displayed in three different colors. The slots shown in grey control the current flows on this layer. These electric elements are made reconfigurable by the inclusion of a set of three PIN diodes connecting these sectors in pairs. There are three additional pairs of straight rectangular slots that reside below the legs of the driven tripole element. A coil inductor is installed at each inner end of the conducting strip formed by the slot pairs to block the RF signal from entering into the DC bias network. Each of the outer ends of these strips is used as the connection point for the DC feeder lines required to control the states of the diodes. The gaps between the sectors are equal. Pattern reconfigurability is obtained by appropriately switching particular diodes on or off. With slight overlaps of each 120° sector, the entire 360° azimuth range is covered.

The multi-layer system was fabricated, assembled, and tested [66]. The realized prototype is shown in Fig. 18. The experimental and simulation results were in good agreement. The measured performance characteristics indicated that in each of its instantaneous states, the antenna at its resonance frequency, 1.564 GHz, produces uniform peak realized gains, front-to-back ratios, and radiation efficiencies. They are, respectively, as high as 3.55 dBi, 17.5 dB, and 84.9%, even though the entire system is electrically small: $ka = 0.92$, and low profile: 0.05 λ_0. The pictured balun was introduced only for measurement purposes to mitigate any leakage currents on the long coax feedline associated with the measurement chamber.

V. RECONFIGURABLE FEEDING NETWORK-ENABLED RECONFIGURABLE ANTENNAS

Reconfigurable feeding networks are another technology that facilitates polarization reconfigurable antennas (RAs) and pattern RAs. For instance, a T-junction power divider and a pair of varactor diodes enable the polarization reconfigurable square-ring microstrip antenna reported in [67]. This configuration produced polarization states that can be switched among an LP and two CP states across an overlapped bandwidth of 1.4% around 2.0 GHz with a maximum realized gain of 7.2 dB. A branch-line coupler with four microstrip feed lines provided the feeding network for the aperture-fed

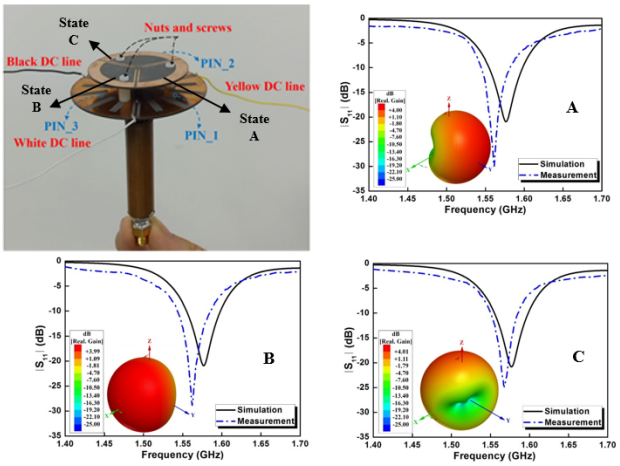

FIGURE 18. The fabricated reconfigurable ESA prototype. The antenna is shown mounted on a semi-rigid coaxial feedline with a sleeve balun installed to mitigate cable currents during the measurements. The measured and simulated $|S_{11}|$ results for each of its three 120° sector coverage states: A, B, and C, show good agreement. The insets are the simulated 3D realized gain patterns at 1.577 GHz, the simulated resonance frequency [66].

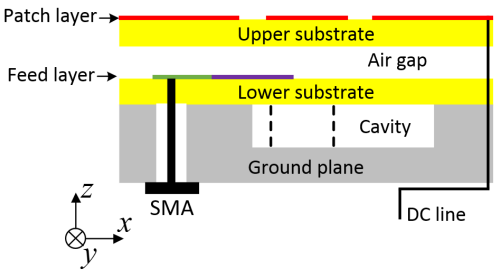

FIGURE 19. Configuration of the reported cavity-backed microstrip reconfigurable antenna [69].

square patch antenna reported in [68]. The feeding network was augmented with eight PIN diodes to provide quadri-polarization reconfigurability, i.e., the polarization could be switched among two orthogonal LP and two orthogonal CP states. An impedance bandwidth of 3.67% at 2.45 GHz with a 5.0 dB realized gain was obtained. A traditional annular slot antenna was modified by introducing an arrow-shaped coupling strip with a PIN diode inserted in each arm [30]. This RA system achieved a wider, 4.7% fractional bandwidth with maximum measured gains around 4.1 dB.

The cavity-backed proximity-coupled reconfigurable microstrip patch antenna illustrated in Fig. 19 realizes both polarization switching and beam steering in a compact configuration [69]. The structure consists of an upper and lower substrate, and a cavity-backed ground plane. The latter is the bottom layer. Its presence and particular shape expedites the impedance matching. The feeding network is printed on top of the lower substrate and the radiating copper patch is printed on the top of the upper substrate, as shown in Fig. 20. Three LP states along the $\phi = 0°$, $\phi = 45°$, and $\phi = 90°$ directions are reconfigured simply by controlling the two

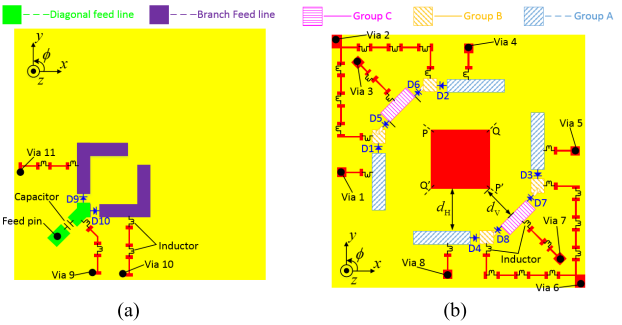

FIGURE 20. The feeding network facilitates the reconfigurability of the cavity-backed microstrip RA. (a) Top view of the feed layer. (b) Top view of the patch layer [69].

diodes D9 and D10 inserted, as shown in Fig. 20 (a), into the feeding network. They connect or disconnect the diagonal and the two branch feeding lines. More specifically, when D9 is ON and D10 is OFF, the $\phi = 0°$ LP state is aligned with the x-axis. Similarly, the $\phi = 90°$ LP state is aligned along y-axis when D9 is OFF and D10 is ON. When both D9 and D10 are ON, the LP state is along the 45° diagonal line.

Beam steering is realized for each of these three polarization states by reconfiguring the parasitic lines to be aligned with the specific polarization direction. For example, as illustrated in Fig. 20 (b), the active parasitic lines for the y-polarized ($\phi = 90°$) state are those of groups A and B that are printed vertically and contain the PIN diodes D1 and D3. The two active parasitic lines have the same length (L1) when both of these diodes are OFF (and all of the other diodes are also OFF). The main beam then points towards the broadside direction. When D3 is ON and D1 is OFF, the right active parasitic line (with length of L1 + L2) is longer than the left one (L1). The main beam then steers to the $-x$-axis direction (left beam). When D3 is OFF and D1 is ON, the beam is steered to the $+x$-axis direction (right beam). Thus, for each of these three polarization states, three reconfigurable beams are obtained by using the reconfigurable parasitic-element network. Overall, the antenna exhibits nine reconfigurable working modes (states), as shown in Table 1.

The measured and simulated $|S_{11}|$ values at 11.0 GHz for each mode are presented in Fig. 21. The reflection coefficients are all below -10 dB. For each of them, the main beam can be steered in the H-plane amongst the directions $\theta \approx 20°$, $0°$, $-20°$, with $\theta = 0°$ being the broadside direction. The measured realized gains range from 7.2 to 8.1 dBi.

There are additional methodologies that have been reported to realize pattern/beam RAs using controllable feeding networks. Beam steering over 360° in the azimuth plane has been achieved [70] with a four-element L-shaped antenna array. A reconfigurable feeding network was used to select one or two L-shaped slots in order to switch the beam patterns. In the same manner, beam-switching antenna arrays have been developed [26], [71] that employ feeding networks

TABLE 1. Nine operating modes of the antenna.

Operating Mode	Diode Switched ON	Polarization	Pattern
Mode 1	D9	0°	Broadside
Mode 2	D9 D2	0°	Left (-y)
Mode 3	D9 D4	0°	Right (+y)
Mode 4	D10	90°	Broadside
Mode 5	D10 D3	90°	Left (-x)
Mode 6	D10 D1	90°	Right (+x)
Mode 7	D9 D10	45°	Broadside
Mode 8	D9 D10 D7 D8	45°	Left (-x and +y)
Mode 9	D9 D10 D5 D6	45°	Right (+x and -y)

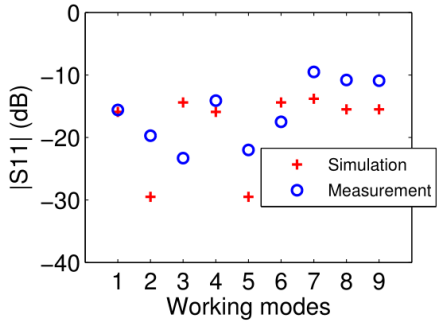

FIGURE 21. Simulated and measured $|S_{11}|$ values at 11.0 GHz for all nine working modes [69].

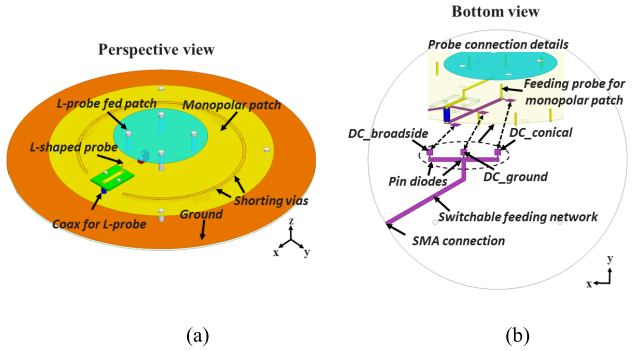

FIGURE 22. Geometry of the PRA that can switch between broadside and conical beams. (a) Perspective view. (b) Reconfigurable feeding network [72].

which are integrated with reconfigurable defected microstrip structure (RDMS) phase shifters. The beam can be steered among the directions: −15°, 0°, 15° with respect to broadside, by changing the phase difference between the array elements.

The wideband pattern RA with switchable broadside and conical beams illustrated in Fig. 22 (a) has been realized recently [72]. It consists of three parts: an L-probe fed patch antenna, a center-fed monopolar patch antenna, and a

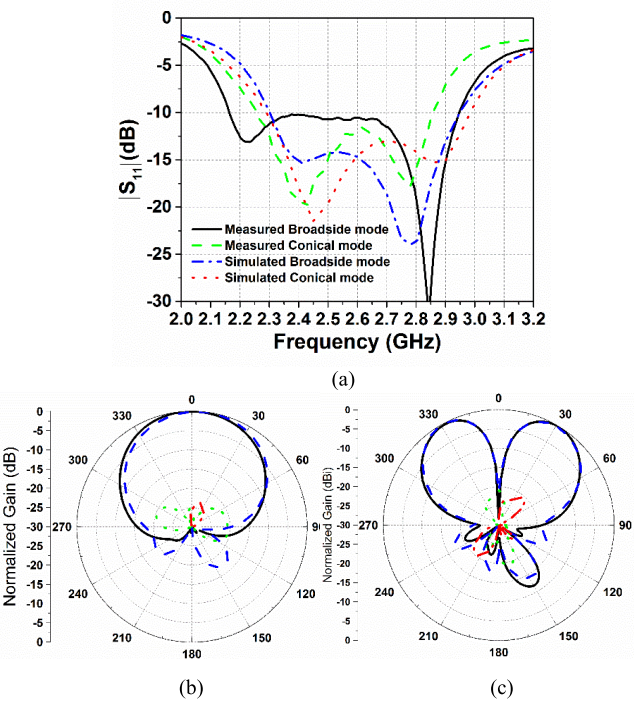

FIGURE 23. Broadside and conical beam RA. (a) Simulated and measured input reflection coefficients. (b) Measured radiation patterns in the two orthogonal vertical planes for both the broadside (left) and conical (right) radiation modes at 2.55 GHz [72].

reconfigurable feeding network. The broadside and conical radiating modes are realized with the reconfigurable feeding network displayed in Fig. 22 (b). This arrangement facilitates the selection of the current paths that excite either the monopolar patch or the L-probe fed patch. The measured and simulated input reflection coefficients are compared in Fig. 23 (a). Very nice agreement between the measured and simulated results was obtained. The measured overlapping $|S_{11}| < -10$-dB fractional impedance bandwidth is 23.5% from 2.25 to 2.85 GHz. The measured radiation patterns in the two orthogonal vertical planes for both the broadside and conical radiation modes at 2.55 GHz are shown in Fig. 23 (b).

For applications like satellite communications, CP radiation performance is desired. However, most pattern reconfigurable antennas reported to date have been linearly-polarized. The realization of CP pattern reconfigurability between broadside and conical modes is quite challenging. Reconfigurable feeding networks can overcome many of the issues that hamper realizing this feature. In particular, a CP pattern reconfigurable microstrip antenna was developed in [73] with a reported 1.6% fractional impedance bandwidth and a maximum 4.0 dBic realized gain. The novel reconfigurable feeding network depicted in Fig. 24 led to a significant improvement of the bandwidth and gain [74]. This design facilitates switching between two sets of excitations of the TM_{11} and TM_{21} modes of the slotted-patch. This produces the CP broadside and conical beams illustrated in Fig. 25. The realized operating fractional bandwidth was 7.8%, which is

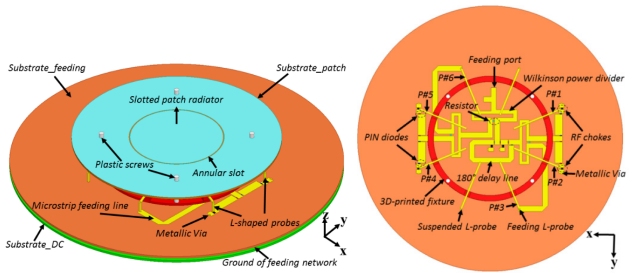

FIGURE 24. Geometry of the PRA with CP switchable broadside and conical beams. (a) Perspective view. (b) Top view of the reconfigurable feeding network [74].

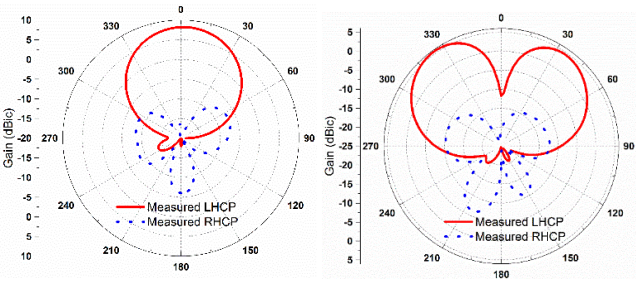

FIGURE 25. Measured radiation patterns of the CP beam reconfigurable antenna for its (a) broadside and (b) conical modes at 2.5 GHz [74].

4.8 times wider than the original design in [73]. The measured peak realized gain was 8.5 dBic and 5.8 dBic for the broadside and conical modes, respectively.

VI. CONCLUSIONS

Several classes of reconfigurable antennas (RAs) enabled by new technologies were reviewed. Examples of recently reported reconfigurable partially reflective surface (PRS) antennas, reconfigurable filtennas, reconfigurable Huygens dipole antennas, and reconfigurable feeding network-enabled antennas were presented. They represent classes of frequency, pattern, polarization, and beam-direction reconfigurable systems realized by innovative combinations of radiating structures and circuit components. Measured results validate their simulated performance characteristics. These RAs and future extensions have the great potential to provide many performance characteristics desired to enhance current wireless platforms and to enable future cognitive radio and other 5G and beyond wireless systems.

It is worth noting that, to date, research on RAs has been mainly focused on innovations in antenna structures and their feeding mechanisms. Whilst these endeavors will undoubtedly continue, future research in this field will also need to focus on issues that are of critical importance to practical systems. These features include wideband operation, gain enhancement and reconfiguration mechanisms to handle high power, while themselves being low power consumers. Since many current and future antenna systems for communications and sensing necessarily employ antenna arrays, reconfigurable antenna arrays with acceptable complexity serve as another important research direction for future endeavors.

REFERENCES

[1] J. Volakis, *Antenna Engineering Handbook*, 4th ed. New York, NY, USA: McGraw-Hill, 2007.

[2] J. H. Reed, J. T. Bernhard, and J.-M. Park, "Spectrum access technologies: The past, the present, and the future," *Proc. IEEE*, vol. 100, no. 5, pp. 1676–1684, May 2012.

[3] J. T. Bernhard, *Reconfigurable Antennas*. San Rafael, CA, USA: Morgan & Claypool, 2007.

[4] J. T. Bernhard, "Reconfigurable antennas," in *Antenna Engineering Handbook*, J. L. Volakis, 4th ed. New York, NY, USA: McGraw-Hill, 2007.

[5] Y. J. Guo and P.-Y. Qin, "Reconfigurable antennas for wireless communications," in *Handbook of Antenna Technologies*, Z. N. Chen, Ed. Berlin, Germany: Springer, 2016.

[6] A. P. Feresidis and J. C. Vardaxoglou, "High gain planar antenna using optimised partially reflective surfaces," *Proc. Inst. Elect. Eng., Antennas Propag.*, vol. 148, no. 6, pp. 345–350, Dec. 2001.

[7] G. V. Trentini, "Partially reflecting sheet arrays," *IRE Trans. Antennas Propag.*, vol. 4, no. 4, pp. 666–671, Oct. 1956.

[8] A. R. Weily, T. S. Bird, and Y. J. Guo, "A reconfigurable high-gain partially reflecting surface antenna," *IEEE Trans. Antennas Propag.*, vol. 56, no. 11, pp. 3382–3390, Nov. 2008.

[9] J. Perruisseau-Carrier, "Dual-polarized and polarization-flexible reflective cells with dynamic phase control," *IEEE Trans. Antenna Propag.*, vol. 58, no. 5, pp. 1494–1502, May 2010.

[10] H. L. Zhu, S. W. Cheung, X. H. Liu, and T. I. Yuk, "Design of polarization reconfigurable antenna using metasurface," *IEEE Trans. Antennas Propag.*, vol. 62, no. 6, pp. 2891–2898, Jun. 2014.

[11] A. Ourir, S. N. Burokur, and A. de Lustrac, "Phase-varying metamaterial for compact steerable directive antenna," *Electron. Lett.*, vol. 43, no. 9, pp. 493–494, Apr. 2007.

[12] A. Ourir, S. N. Burokur, and A. de Lustrac, "Electronic beam steering of an active metamaterial-based directive subwavelength cavity," in *Proc. 2nd Eur. Conf. Antennas Propag.*, Edinburgh, Scotland, Nov. 2007, pp. 1–4.

[13] T. Debogovic and J. Perruisseau-Carrier, "Array-fed partially reflective surface antenna with independent scanning and beamwidth dynamic control," *IEEE Trans. Antennas Propag.*, vol. 62, no. 1, pp. 446–449, Jan. 2014.

[14] A. P. Feresidis, G. Goussetis, S. Wang, and J. C. Vardaxoglou, "Artificial magnetic conductor surfaces and their application to low-profile high-gain planar antennas," *IEEE Trans. Antennas Propag.*, vol. 53, no. 1, pp. 209–215, Jan. 2005.

[15] S. Wang, A. P. Feresidis, G. Goussetis, and J. C. Vardaxoglou, "High-gain subwavelength resonant cavity antennas based on metamaterial ground planes," *Proc. Inst. Elect. Eng., Microw. Antennas Propag.*, vol. 153, no. 1, pp. 1–6, Feb. 2006.

[16] P.-Y. Qin, Y. J. Guo, A. R. Weily, and C.-H. Liang, "A pattern reconfigurable U-slot antenna and its applications in MIMO systems," *IEEE Trans. Antennas Propag.*, vol. 60, no. 2, pp. 516–528, Feb. 2012.

[17] C. Gu *et al.*, "Compact smart antenna with electronic beam-switching and reconfigurable polarizations," *IEEE Trans. Antennas Propag.*, vol. 63, no. 12, pp. 5325–5333, Dec. 2015.

[18] Y. Li, Z. Zhang, J. Zheng, Z. Feng, and M. F. Iskander, "Experimental analysis of a wideband pattern diversity antenna with compact reconfigurable CPW-to-slotline transition feed," *IEEE Trans. Antennas Propag.*, vol. 59, no. 11, pp. 4222–4228, Nov. 2011.

[19] S. Zhang, G. H. Huff, J. Feng, and J. T. Bernhard, "A pattern reconfigurable microstrip parasitic array," *IEEE Trans. Antennas Propag.*, vol. 52, no. 10, pp. 2773–2776, Oct. 2004.

[20] X. S. Yang, B. Z. Wang, W. Wu, and S. Xiao, "Yagi patch antenna with dual-band and pattern reconfigurable characteristics," *IEEE Antennas Wireless Propag. Lett.*, vol. 6, pp. 168–171, 2007.

[21] C. Gu *et al.*, "Dual-band electronically beam-switched antenna using slot active frequency selective surface," *IEEE Trans. Antennas Propag.*, vol. 65, no. 3, pp. 1393–1398, Mar. 2017.

[22] R. Guzman-Quiros, J. L. Gomez-Tornero, A. R. Weily, and Y. J. Guo, "Electronically steerable 1-D Fabry–Perot leaky-wave antenna employing a tunable high impedance surface," *IEEE Trans. Antennas Propag.*, vol. 60, no. 11, pp. 5046–5055, Nov. 2012.
[23] R. Guzmán-Quirós, J. L. Gómez-Tornero, A. R. Weily, and Y. J. Guo, "Electronic full-space scanning with 1-D Fabry–Pérot LWA using electromagnetic band-gap," *IEEE Antennas Wireless Propag. Lett.*, vol. 11, pp. 1426–1429, 2012.
[24] R. Guzmán-Quirós, J. L. Gómez-Tornero, A. R. Weily, and Y. J. Guo, "A Fabry–Pérot antenna with two-dimensional electronic beam scanning," *IEEE Trans. Antennas Propag.*, vol. 64, no. 4, pp. 1536–1541, Apr. 2016.
[25] L. Y. Ji, Y. J. Guo, P. Y. Qin, S. X. Gong, and R. Mittra, "A reconfigurable partially reflective surface (PRS) antenna for beam steering," *IEEE Trans. Antennas Propag.*, vol. 63, no. 6, pp. 2387–2395, Jun. 2015.
[26] C. Ding, Y. J. Guo, P.-Y. Qin, T. S. Bird, and Y. Yang, "A defected microstrip structure (DMS)-based phase shifter and its application to beamforming antennas," *IEEE Trans. Antennas Propag.*, vol. 62, no. 2, pp. 641–651, Feb. 2014.
[27] Y. Li, Z. Zhang, W. Chen, and Z. Feng, "Polarization reconfigurable slot antenna with a novel compact CPW-to-slotline transition for WLAN application," *IEEE Antennas Wireless Propag. Lett.*, vol. 13, pp. 579–582, 2014.
[28] H. Wong, W. Lin, L. Huitema, and E. Arnaud, "Multi-polarization reconfigurable antenna for wireless biomedical system," *IEEE Trans. Biomed. Circuits Syst.*, vol. 11, no. 3, pp. 652–660, Jun. 2017.
[29] W. Lin and H. Wong, "Wideband circular polarization reconfigurable antenna," *IEEE Trans. Antennas Propag.*, vol. 63, no. 12, pp. 5938–5944, Dec. 2015.
[30] J.-S. Row, W.-L. Liu, and T.-R. Chen, "Circular polarization and polarization reconfigurable designs for annular slot antennas," *IEEE Trans. Antennas Propag.*, vol. 60, no. 12, pp. 5998–6002, Dec. 2012.
[31] W. Lin and H. Wong, "Polarization reconfigurable wheel-shaped antenna with conical-beam radiation pattern," *IEEE Trans. Antennas Propag.*, vol. 63, no. 2, pp. 491–499, Feb. 2015.
[32] W. Lin and H. Wong, "Polarization reconfigurable aperture-fed patch antenna and array," *IEEE Access*, vol. 4, pp. 1510–1517, 2016.
[33] W. Han, J. OuYang, Z. Guo, Y. Li, and F. Yang, "A single-feed high-gain fabry-perot antenna with reconfigurable polarization capability," in *Proc. Cross Strait Quad-Regional Radio Sci. Wireless Technol. Conf.*, Chengdu, China, Jul. 2013, pp. 279–281.
[34] L.-Y. Ji, P.-Y. Qin, Y. J. Guo, C. Ding, and S.-X. Gong, "A wideband polarization reconfigurable antenna with partially reflective surface," *IEEE Trans. Antennas Propag.*, vol. 64, no. 10, pp. 4534–4538, Oct. 2016.
[35] G. J. K. Moernaut and G. A. E. Vandenbosch, "Concept study of a shorted annular patch antenna: Design and fabrication on a conducting cylinder," *IEEE Trans. Antennas Propag.*, vol. 59, no. 6, pp. 2097–2102, Jun. 2011.
[36] J. Mitola and G. Q. Maguire, Jr., "Cognitive radio: Making software radios more personal," *IEEE Pers. Commun.*, vol. 6, no. 4, pp. 13–18, Apr. 1999.
[37] S. V. Hum and H. Y. Xiong, "Analysis and design of a differentially-fed frequency agile microstrip patch antenna," *IEEE Trans. Antennas Propag.*, vol. 58, no. 10, pp. 3122–3130, Oct. 2010.
[38] S. Genovesi, A. Di Candia, and A. Monorchio, "Compact and low profile frequency agile antenna for multistandard wireless communication systems," *IEEE Trans. Antennas Propag.*, vol. 62, no. 3, pp. 1019–1026, Mar. 2014.
[39] P.-Y. Qin, A. R. Weily, Y. J. Guo, T. S. Bird, and C.-H. Liang, "Frequency reconfigurable quasi-Yagi folded dipole antenna," *IEEE Trans. Antennas Propag.*, vol. 58, no. 8, pp. 2742–2747, Aug. 2010.
[40] F. Ghanem, P. S. Hall, and J. R. Kelly, "Two port frequency reconfigurable antenna for cognitive radios," *Electron. Lett.*, vol. 45, no. 11, pp. 534–536, May 2009.
[41] T. Aboufoul, A. Alomainy, and C. Parini, "Reconfiguring UWB monopole antenna for cognitive radio applications using GaAs FET switches," *IEEE Antennas Wireless Propag. Lett.*, vol. 11, pp. 392–394, 2012.
[42] M. R. Hamid, P. Gardner, P. S. Hall, and F. Ghanem, "Vivaldi antenna with integrated switchable band pass resonator," *IEEE Trans. Antennas Propag.*, vol. 59, no. 11, pp. 4008–4015, Nov. 2011.
[43] P.-Y. Qin, Y. J. Guo, and F. Wei, "A wideband-to-narrowband tunable antenna using a reconfigurable filter," *IEEE Trans. Antennas Propag.*, vol. 63, no. 5, pp. 2282–2285, May 2015.
[44] J. T. Kuo and E. Shih, "Wideband bandpass filter design with three-line microstrip structures," *Proc. Inst. Elect. Eng., Microw. Antennas Propag.*, vol. 149, no. 56, pp. 243–247, Oct. 2002.
[45] M.-C. Tang, Z. Wen, H. Wang, M. Li, and R. W. Ziolkowski, "Compact, frequency-reconfigurable filtenna with sharply defined wideband and continuously tunable narrowband states," *IEEE Trans. Antennas Propag.*, vol. 65, no. 10, pp. 5026–5034, Oct. 2017.
[46] J.-S. Hong and M. J. Lancaster, *Microstrip Filters for RF/Microwave Applications*. New York, NY, USA: Wiley, 2001.
[47] K. Srisathit and W. Surakumpontorn, "Wideband microstrip bandpass filter based on modified parallel-coupled line topology," in *Proc. 10th Int. Symp. Commun. Inf. Technol.*, Tokyo, Japan, Oct. 2010, pp. 45–48.
[48] R. W. Ziolkowski, P. Jin, and C.-C. Lin, "Metamaterial-inspired engineering of antennas," *Proc. IEEE*, vol. 99, no. 10, pp. 1720–1731, Oct. 2011.
[49] R. T. Cutshall and R. W. Ziolkowski, "Performance characteristics of planar and three-dimensional versions of a frequency-agile electrically small antenna," *IEEE Antennas Propag. Mag.*, vol. 56, no. 6, pp. 53–71, Dec. 2014.
[50] M.-C. Tang, R. W. Ziolkowski, S. Xiao, M. Li, and J. Zhang, "Frequency-agile, efficient, near-field resonant parasitic monopole antenna," *IEEE Trans. Antennas Propag.*, vol. 62, no. 3, pp. 1479–1483, Mar. 2014.
[51] M.-C. Tang and R. W. Ziolkowski, "Frequency-agile, efficient, circularly polarized, near-field resonant antenna: Designs and measurements," *IEEE Trans. Antennas Propag.*, vol. 63, no. 11, pp. 5203–5209, Nov. 2015.
[52] N. Zhu, R. W. Ziolkowski, and H. Xin, "A metamaterial-inspired, electrically small rectenna for high-efficiency low power harvesting and scavenging at the GPS L1 frequency," *Appl. Phys. Lett.*, vol. 99, p. 114101, Sep. 2011.
[53] N. Zhu, R. W. Ziolkowski, and H. Xin, "Electrically small GPS L1 rectennas," *IEEE Antennas Wireless Propag. Lett.*, vol. 10, pp. 935–938, 2011.
[54] P. Jin and R. W. Ziolkowski, "Broadband, efficient, electrically small metamaterial-inspired antennas facilitated by active near-field resonant parasitic elements," *IEEE Trans. Antennas Propag.*, vol. 58, no. 2, pp. 318–327, Feb. 2010.
[55] N. Zhu and R. W. Ziolkowski, "Design and measurements of an electrically small, broad bandwidth, non-Foster circuit-augmented protractor antenna," *Appl. Phys. Lett.*, vol. 101, p. 024107, Jul. 2012.
[56] N. Zhu and R. W. Ziolkowski, "Broad-bandwidth, electrically small antenna augmented with an internal non-foster element," *IEEE Antennas Wireless Propag. Lett.*, vol. 11, pp. 1116–1120, 2012.
[57] N. Zhu and R. W. Ziolkowski, "Broad bandwidth, electrically small, non-Foster element-augmented antenna designs, analyses, and measurements," *IEICE Trans. Commun.*, vol. E96-B, no. 10, pp. 2399–2409, Oct. 2013.
[58] M.-C. Tang, N. Zhu, and R. W. Ziolkowski, "Augmenting a modified egyptian axe dipole antenna with non-foster elements to enlarge its directivity bandwidth," *IEEE Antennas Wireless Propag. Lett.*, vol. 12, pp. 421–424, 2013.
[59] P. Jin and R. W. Ziolkowski, "Metamaterial-inspired, electrically small huygens sources," *IEEE Antennas Wireless Propag. Lett.*, vol. 9, pp. 501–505, 2010.
[60] R. W. Ziolkowski, "Low profile, broadside radiating, electrically small huygens source antennas," *IEEE Access*, vol. 3, pp. 2644–2651, 2015.
[61] M.-C. Tang, H. Wang, and R. W. Ziolkowski, "Design and testing of simple, electrically small, low-profile, huygens source antennas with broadside radiation performance," *IEEE Trans. Antennas Propag.*, vol. 64, no. 11, pp. 4607–4617, Nov. 2016.
[62] M.-C. Tang, T. Shi, and R. W. Ziolkowski, "A study of 28 GHz, planar, multilayered, electrically small, broadside radiating, huygens source antennas," *IEEE Trans. Antennas Propag.*, vol. 65, no. 12, pp. 6345–6354, Dec. 2017.
[63] W. Lin and R. W. Ziolkowski, "Electrically-small, low-profile, huygens circularly polarized antenna," *IEEE Trans. Antennas Propag.*, to be published, doi: 10.1109/TAP.2017.2784432.
[64] R. W. Ziolkowski, M.-C. Tang, and N. Zhu, "An efficient, broad bandwidth, high directivity, electrically small antenna," *Microw. Opt. Technol. Lett.*, vol. 55, no. 6, pp. 1430–1434, Jun. 2013.
[65] M.-C. Tang, T. Shi, and R. W. Ziolkowski, "Electrically small, broadside radiating huygens source antenna augmented with internal non-foster elements to increase its bandwidth," *IEEE Antennas Wireless Propag. Lett.*, vol. 16, pp. 712–715, 2017.
[66] M.-C. Tang, B. Zhou, and R. W. Ziolkowski, "Low-profile, electrically small, huygens source antenna with pattern-reconfigurability that covers the entire azimuthal plane," *IEEE Trans. Antennas Propag.*, vol. 65, no. 3, pp. 1063–1072, Mar. 2017.
[67] J. F. Tsai and J. S. Row, "Reconfigurable square-ring microstrip antenna," *IEEE Trans. Antennas Propag.*, vol. 61, no. 5, pp. 2857–2860, May 2013.

[68] Y. F. Wu, C. H. Wu, D. Y. Lai, and F. C. Chen, "A reconfigurable quadri-polarization diversity aperture-coupled patch antenna," *IEEE Trans. Antennas Propag.*, vol. 55, no. 3, pp. 1009–1012, Mar. 2007.
[69] S.-L. Chen, P.-Y. Qin, C. Ding, and Y. J. Guo, "Cavity-backed proximity-coupled reconfigurable microstrip antenna with agile polarizations and steerable beams," *IEEE Trans. Antennas Propag.*, vol. 65, no. 10, pp. 5553–5558, Oct. 2017.
[70] M.-I. Lai, T.-Y. Wu, J.-C. Hsieh, C.-H. Wang, and S.-K. Jeng, "Compact switched-beam antenna employing a four-element slot antenna array for digital home applications," *IEEE Trans. Antennas Propag.*, vol. 56, no. 9, pp. 2929–2936, Sep. 2008.
[71] C. Ding, Y. J. Guo, P.-Y. Qin, and Y. Yang, "A compact microstrip phase shifter employing reconfigurable defected microstrip structure (RDMS) for phased array antennas," *IEEE Trans. Antennas Propag.*, vol. 63, no. 5, pp. 1985–1996, May 2015.
[72] W. Lin, H. Wong, and R. W. Ziolkowski, "Wideband pattern-reconfigurable antenna with switchable broadside and conical beams," *IEEE Antennas Wireless Propag. Lett.*, vol. 16, pp. 2638–2641, 2017.
[73] N. R. Labadie, S. K. Sharma, and G. M. Rebeiz, "A circularly polarized multiple radiating mode microstrip antenna for satellite receive applications," *IEEE Trans. Antennas Propag.*, vol. 62, no. 7, pp. 3490–3500, Jul. 2014.
[74] W. Lin, H. Wong, and R. W. Ziolkowski, "Reconfigurable patch antenna with switchable broadside and conical circularly-polarized radiation patterns," *IEEE Trans. Antennas Propag.*, to be published, doi: 10.1109/TAP.2017.2784452.

Y. JAY GUO (F'14) received the bachelor's and master's degrees from Xidian University, China, in 1982 and 1984, respectively, and the Ph.D. degree from Xi'an Jiaotong University in 1987.

He is currently a Distinguished Professor and the Founding Director with the Global Big Data Technologies Centre, University of Technology Sydney, Australia. Prior to this appointment in 2014, he served as a Director with Commonwealth Scientific and Industrial Research Organisation (CSIRO) for over nine years, directing a number of ICT research portfolios. Before joining CSIRO, he held various senior leadership positions with Fujitsu, Siemens, and NEC in the U.K. His research interests include antennas, mm-wave and THz communications, and sensing systems as well as big data.

Dr. Guo has chaired numerous international conferences. He was the International Advisory Committee Chair of the IEEE VTC2017, General Chair of ISAP2015, iWAT2014, and WPMC'2014, and a TPC Chair of 2010 IEEE WCNC, and 2012 and 2007 IEEE ISCIT. He served as a Guest Editor of special issues on Antennas for Satellite Communications and Antennas and Propagation Aspects of 60-90GHz Wireless Communications, both in the IEEE TRANSACTIONS ON ANTENNAS AND PROPAGATION, Special Issue on Communications Challenges and Dynamics for Unmanned Autonomous Vehicles, the IEEE JOURNAL ON SELECTED AREAS IN COMMUNICATIONS, and Special Issue on 5G for Mission Critical Machine Communications, the *IEEE Network Magazine*. He is currently a Fellow of the Australian Academy of Engineering and Technology, a Fellow of IET, and a member of the College of Experts of Australian Research Council. He has won a number of most prestigious Australian national awards, and was named one of the most influential engineers in Australia in 2014 and 2015. He has authored over 350 research papers and holds 22 patents in antennas and wireless systems.

PEI-YUAN QIN (M'13) was born in Liaoning Province, China, in 1983. He received the bachelor's degree in electronic engineering from Xidian University, Xi'an, China, in 2006, and the joint Ph.D. degree in electromagnetic fields and microwave technology from Xidian University and Macquarie University, Australia, in 2012.

From 2012 to 2015, he was a Post-Doctoral Research Fellow with Commonwealth Scientific and Industrial Research Organisation (CSIRO), Australia. From 2015 to 2016, he was a Chancellor's Post-Doctoral Research Fellow/Lecturer with the University of Technology Sydney (UTS), Australia. Since 2017, he has been a Senior Lecturer with UTS. His research interests are in the areas of reconfigurable antennas, phase shifters, reconfigurable reflect arrays, and MIMO communications.

Dr. Qin was a recipient of an Australia Research Council Discovery Early Career Researcher Award and also a recipient of the International Macquarie University Research Excellence Scholarship and was awarded the Vice Chancellor's Commendation for academic excellence by Macquarie University. One of his papers was selected as 2016 Computer Simulation Technology University Publication Award. Since 2017, he has been serving as an Associate Editor of the IEEE ANTENNAS AND WIRELESS PROPAGATION LETTERS.

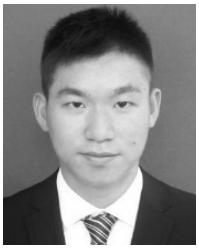

SHU-LIN CHEN (S'16) was born in Hubei Province, China. He received the B.S. degree in electrical engineering from Fuzhou University, China, in 2012, and the M.S. degree in electromagnetic field and microwave technology from Xiamen University, China, in 2015. Since 2016, he has been currently pursuing the Ph.D. degree in engineering with the Global Big Data Technologies Centre, University of Technology Sydney, Australia.

WEI LIN received the bachelor's and master's degrees in electronic engineering from the South China University of Technology, Guangzhou, China, in 2009 and 2012, respectively, and the Ph.D. degree in electronic engineering from the City University of Hong Kong, Hong Kong, in 2016.

He was a Research Associate with Nanyang Technological University, Singapore, from 2012 to 2013. He is currently a Post-Doctoral Research Fellow with the Global Big Data Technologies Centre, University of Technology Sydney, Ultimo NSW, Australia. His research interests include the designs of reconfigurable antennas, HF antennas, satellite antennas, millimeter wave antennas, terahertz devices, and their applications. Mr. Lin was awarded the Outstanding Master Thesis Award from South China University of Technology in 2013. He was a recipient of the Young Scientist Award at the IEEE Region 10 conference (TENCON) in 2015, a Talent Development Scholarship from the Hong Kong SAR Government in 2016, the best poster paper award in the Second international conference on Electromagnetic Materials and Technologies for the Future (EM-MTF2017) in 2017, and the UTS Early Career Researcher Grant Award from University of Technology Sydney commencing 2018. He serves as a reviewer for many IEEE and IET journals.

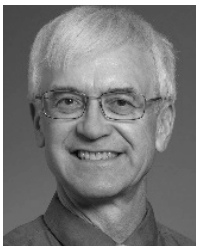

RICHARD W. ZIOLKOWSKI received the B.Sc. *(magna cum laude)* degree from Brown University, Providence, RI, USA, in 1974, and the M.S. and Ph.D. degrees from the University of Illinois at Urbana–Champaign, Urbana, IL, USA, in 1975 and 1980, respectively, all in physics, and the Honorary Doctorate degree from the Technical University of Denmark, Kongens Lyngby, Denmark, in 2012.

He is currently a Distinguished Professor with the Global Big Data Technologies Centre, University of Technology Sydney, Ultimo NSW, Australia, and also a Litton Industries John M. Leonis Distinguished Professor with the Department of Electrical and Computer Engineering and a Professor with the College of Optical Sciences, The University of Arizona. He was the Computational Electronics and Electromagnetics Thrust Area Leader with the Lawrence Livermore National Laboratory, Engineering Research Division, before joining The University of Arizona, Tucson, AZ, USA, in 1990. He was the Australian DSTO Fulbright Distinguished Chair with the Advanced Science and Technology from 2014 to 2015. He was a 2014 Thomas-Reuters Highly Cited Researcher. His current research interests include the application of new mathematical and numerical methods to linear and nonlinear problems dealing with the interaction of electromagnetic and acoustic waves with complex linear and nonlinear media, as well as metamaterials, metamaterial-inspired structures, and applications-specific configurations.

Dr. Ziolkowski is currently a Fellow of the Optical Society of America, 2006, and the American Physical Society, 2016. He served as the President of the IEEE Antennas and Propagation Society in 2005. He is also actively involved with the URSI, OSA, and SPIE professional societies.